INDIAN JOURNAL OF SCIENCE AND TECHNOLOGY

ORIGINAL ARTICLE

# Synergistic Mechanisms Indigo Carmine Removal using Clay Rich Iron Coupled Ultrasound and Oxidant

**Mahamadou Kamagate[1]*, Traoré Lanciné[1], Coulibaly Gnougon Nina[1], Coulibaly Lacina[2]**

**1** UFR Sciences and Technologies, Université de Man BP 20, Man, Côte d'Ivoire
**2** Environmental and Aquatic Biology Laboratory, Université Nangui-Abrogoua, 02 BP 801, Abidjan 02, Cote d'Ivoire

OPEN ACCESS

**Received:** 21/10/2025
**Accepted:** 29/11/2025
**Published:** 30/11/2025

**Citation:** Kamagate M, Lanciné T, Nina CG, Lacina C (2025) Synergistic Mechanisms Indigo Carmine Removal using Clay Rich Iron Coupled Ultrasound and Oxidant. Indian Journal of Science and Technology 18(43): 3396-3405. https ://doi.org/10.17485/IJST/v18i43.1732

* **Corresponding author**.

kamagate.mahamadou@univ-man.edu.ci

**Funding:** None

**Competing Interests:** None

**Copyright:** © 2025 Kamagate et al. This is an open access article distributed under the terms of the Creative Commons Attribution License, which permits unrestricted use, distribution, and reproduction in any medium, provided the original author and source are credited.

Published By Indian Society for Education and Environment (iSee)

**ISSN**
Print: 0974-6846
Electronic: 0974-5645

## Abstract

**Background/Objectives**: The coloured wastewater discharge from industrial sources cause harm to the human health due to these substance toxicities. Indigo dyes are among the most widely used in the dyeing process.This study is intended to achieve suitable approach to remove the dye using a catalytic method. **Methods**: The dye removal involves a natural catalyst and an oxidant coupled with ultrasound. Initially, the catalyst was characterized using analytical techniques, including Fluorescence and Diffractometer X-ray. Subsequently, the isotherm adsorption was modelled. Then, the degradation parameters optimization such as catalyst dose, dye concentration, PDS concentration and pH was investigated. To establish the involvement of $SO_4^{\bullet -}$, $OH^{\bullet}$, and $HO_2^{\bullet}/O_2^{\bullet -}$ radicals in the degradation of IC, BQ, i-PrOH and t-BuOH, a scavenging test was performed using 100 mM of each product. **Findings**: The catalyst revealed the presence of quartz ($SiO_2$), goethite ($\alpha$-$Fe^{II}O(OH)$), kaolinite ($Al_2Si_2O_5(OH)_4$) and ($KA_{l2}(AlSi_3O_{10})(OH)_2$). Elemental chemical analysis demonstrated the presence of significant quantities of iron (48.98%) and silica (29.43%) in the sample. The adsorption phenomenon enabled the modelling of the isotherm, which demonstrated a perfect fit with the Langmuir model, and the determination of the adsorption kinetics, which are second-order. The subsequent analysis of degradation parameters indicated the following optimal conditions: The concentration of the catalyst (IC) was determined to be 30 $\mu$M, the dosage of the catalyst was established as 2 g/L, the concentration of the PS was measured to be 25 $\mu$M, and the pH was adjusted to 6.45. These conditions resulted in 61.35% degradation. The degradation mechanism demonstrated the involvement of various free radicals in the process, most notably sulfate ($SO_4^{\bullet -}$), hydroxyl ($OH^{\bullet}$) and superoxide ($O_2^{\bullet -}$). In conclusion, it was observed that the catalyst demonstrated a satisfactory catalytic capacity across a series of oxidation cycles, with this capacity being maintained until the fifth cycle. **Novelty:** The dye removal innovative process is involving a natural catalyst and an oxidant coupled with ultrasound. The implementation of this process is an effective approach for the dyes treatment in wastewater.

**Keywords:** Indigo Carmine (IC); Peroxydisulfate (PS); Adsorption; Degradation; Innovative Oxidation Process

# 1 Introduction

The issue of access to drinking water is of paramount importance in numerous countries and is frequently associated with economic disadvantage. Despite the abundance of water on Earth, only a small fraction of this is suitable for consumption. Indeed, the Earth's water reserves are estimated to be approximately 1.38 billion $km^3$. It is evident that the vast majority of the world's water resources are comprised of sea and oceanic waters, accounting for 97.2% of the total. In contrast, consumable fresh water constitutes a comparatively negligible proportion, representing a mere 2.8% of the total water on Earth [1]. This resource is heavily used in textile industries, which generate effluents containing micropollutants, including dyes, posing risks to human health and the environment [2]. It is estimated that a considerable quantity of dyes, amounting to 1,000,000 tonnes per year, is released into the environment during the synthesis and dyeing of fabrics [3], with azo dyes accounting for the majority, representing 60-70 % [4]. Conventional water purification methods can be costly and sometimes unsuitable for the treatment of influents.

In order to address the challenge posed by bio-recalcitrant organic compounds in water and the wider environment, there is an urgent need to develop effective and environmentally friendly treatment techniques (e.g. adsorption, advanced oxidation processes (AOP), membrane filtration) [5]. Many researchers around the world are devoting their efforts to developing these processes. The principle of adsorption treatment is to trap dyes using a solid material called an adsorbent. The literature describes other solid materials (clays, zeolites, activated aluminas, peat, biomass, biopolymers, agricultural residues, industrial by-products, etc.) that can be used in water decolourisation processes [6], [7], [8], [9]. AOPs are reliant upon the in situ formation of highly reactive free radicals. These radicals are capable of degrading all organic contaminants present in water, or breaking them down into biologically degradable molecules [7]. These technologies, which are based on the production of radical entities that can be used in wastewater or industrial effluent treatment, transform complex organic molecules into by-products (which are either biodegradable, like the original compounds, or completely mineralised into $CO_2$ and $H_2O$) [8].

In developing countries, such as Côte d'Ivoire, the water situation has become a concern due to the absence of effluent treatment systems in artisanal dyeing workshops and the inadequate functioning of wastewater collection networks.

The objective of this study is to elucidate the adsorption and degradation mechanisms of an innovative process implemented using a natural catalyst, a strong oxidant coupled with ultrasound. Specifically, the aim is to characterize the catalyst (natural soil), understand the adsorption phenomenon, monitor the degradation kinetics of the dyes by varying its concentration, the catalyst dose and the oxidant concentration in order to optimize the treatment system, the degradation mechanism, and the performance of the catalyst.

# 2 Methodology

## 2.1 Chemicals

All chemicals utilized in this study are of analytical purity. These were supplied by Sigma-Aldrich (Saint-Quentin-Fallavier, France) and others by PubChem. Finally, the FerroVerR reagent kits and the LCK 380 kit were supplied by Hach (Loveland, Colorado, USA). The Table 1 provides a comprehensive list of products and their respective details.

**Table 1.** Complete list and chemical product details

| Chemicals | Cas number | Molar mass (g $mol^{-1}$) | Chemical formula |
|---|---|---|---|
| Indigo Carmine | 860-22-0 | 466.36 | $C_{16}H_8N_2Na_2O_8S_2$ |
| Persulfate de sodium | 15092-81-6 | 192.11 | $Na_2S_2O_8$ |
| Tertbutanol | 75-65-0 | 74.12 | $(CH_3)_3COH$ |
| Isopropanol | 67-63-0 | 60 | $C_3H_8O$ |
| Chloroform | 67-66-3 | 119 | $CHCl_3$ |
| Sodium Hydroxide | 1310-73-2 | 40 | NaOH |
| Hydrogen Chloride | 7647-01-0 | 36.46 | HCl |

## 2.2 Collecting and analysing soil

The clay utilized in this study was sourced from Youhoulil, a town situated within the Lopou area of the Dabou district, which serves as the capital of the region (Côte d'Ivoire). The following coordinates delineate the extraction point: The geographical coordinates are 05°21'29"N and 04°31'18"W. The clay blocks were extracted at a depth of 3.2 m [10], [11]. ubsequently, the sample

was pulverised and subjected to a 50 $\mu$m sieve. Thereafter, the targeted fraction was subjected to a rinse with ultrapure water and elevated to a temperature of 50 °C for the purpose of drying. A variety of instruments were utilized to ascertain the physical and surface characteristics of the soil. The equipment employed for this study included an X-ray fluorescence (XRF) instrument (Horiba, MESA-50, Kyoto, Japan), a Scanning Electron Microscope coupled with Energy Dispersive X-ray (SEM-EDX) (Hirox, SH 4000 M, Tokyo, Japan), and an X-Ray Diffraction instrument (GBC Emma, Hampshire, IL, USA). UPW, with a resistivity of 18.2 MΩ cm, was obtained from a Millipore Milli-Q system and utilized in the production of standard solutions and synthetic wastewater.

### 2.3 Tests and analysis of ultrasonic oxidation

The reactor was constructed within a 10 L stainless-steel tank, which measured 15 cm in height, 24 cm in width, and 30 cm in length. The power and frequency of the signal are 240 W and 40 kHz, respectively. All experiments (i.e., sorption and oxidation) were conducted within a 250 mL batch reactor at ambient temperature (28 $\pm$ 2 °C) and a pH of 7 $\pm$ 0.2. Both experiments were conducted at ambient temperature. Initially, the pollutant solutions (i.e., IC) and the catalyst (i.e., clay) were stirred together in the dark for a period of 4 h, with the aim of ensuring complete absorption. In the second experiment, the pollutants, oxidants and catalyst were amalgamated under ultrasound at 200 rpm for an equivalent duration. The temperature of the suspension remained constant throughout the times of the experiments. During experimentation, the pH variation in the samples was meticulously regulated and monitored using a PHS-38W microprocessor pH meter/mV meter/thermometer. In order to maintain the stability of the solution's pH level, HCl and NaOH were utilized at varying concentrations (0.1; 0.01; 1 M). In both cases, 250 mL of IC solution at the appropriate concentration was added, along with an adequate amount of the catalyst. Thereafter, the requisite quantity of oxidant (PS) was introduced to the solution. During the experimental process, 3 mL of the solution was collected at 30-min intervals for analysis. The measurement of IC concentrations was conducted utilizing the UV-6000PC UV/VIS Spectrophotometer (HKNDT, Single Beam Ultraviolet Visible Spectrophotometer, Wavelength Range 190-1100 nm, Bandwidth 1.8 nm with UV VIS Analyst Software). The assessment of degradation percentage for varying treatment times was executed in accordance with the following equation:

$$Degradation\ (\%) = \frac{C0 - Ct}{C0} X\ 100 \quad \text{(Eqn. 1)}$$

Where $C_0$ and Ct represent the initial and the variable-time interval t concentrations of the pollutants, respectively.

TOC Concentration was measured during the reaction using a DR 3900TM spectrophotometer (Hach$^R$) with 10 mL of solution and a pre-programmed method. The study also monitored the level of some heavy metals (e.g. Fe, Cr, Mn, Cu, Co, Ni, and Zn) that could be extracted from the surfaces of the catalyst to the treated solution using the XRF instrument. In order to demonstrate the involvement of $SO_4^{\bullet -}$, $OH^{\bullet}$, and $HO_2^{\bullet}/O_2^{\bullet -}$ radicals in the degradation of IC, BQ, i-PrOH and t-BuOH, a scavenging test was performed using 100 mM of each product. It is evident that the optimum concentration of scavengers for the execution of these experiments was ascertained *via* the method of varying their concentrations from 10 to 100 mM. All experiments were performed thrice and exhibited minimal variation, with a mean standard error of less than 3%.

## 3 Result and discussion

### 3.1 Catalyst Morphology

Figure 1 illustrates images obtained by scanning electron microscopy (SEM) of the catalyst at varying magnifications. This technique is employed to visualise the morphology and to determine the size of the catalyst pores. At 30 $\mu$m, the presence of detached flakes and more visible pores can be observed, as indicated by the parts circled and marked with red arrows. The area delineated in yellow on the provided diagram will be subjected to microanalysis.

### 3.2 Chemical element and oxide of the catalyst

The elemental chemical analysis yielded significant results, indicating the presence of iron (28.98%), followed by silicon (51.43%). The elevated iron and silica content indicates that the catalyst is a ferrosilicate. With regard to oxide composition, the predominant substances identified were iron oxide (26.85%) and silicon oxide (57.34%).

### 3.3 Microanalysis mapping

The preliminary mapping, conducted at a scale of 30 $\mu$m (See Figure 2), substantiates the coexistence of elements O, Al, Si, Ti, Fe and K across all samples. The distribution of the elements oxygen (O), aluminium (Al) and silicon (Si) is almost identical and can

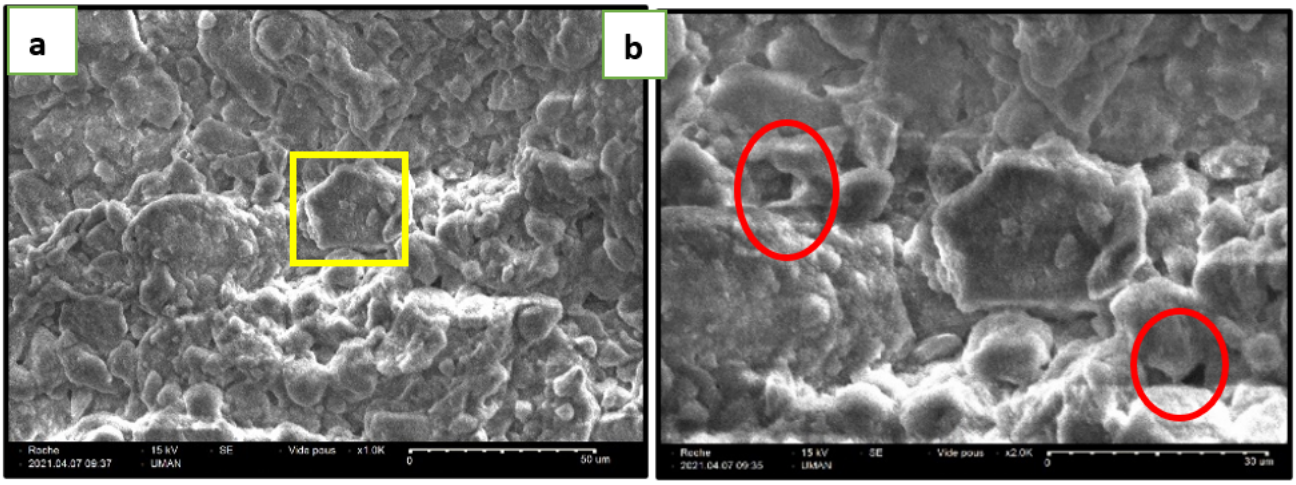


**Fig 1.** Morphology of the catalyst sample at different magnifications using a HIROX SEM, model SH-4000 M. a: 50 $\mu$m and b: 30 $\mu$m

be superimposed. In a similar manner, the distribution of elements Fe and K is almost identical and can also be superimposed to form oxides.

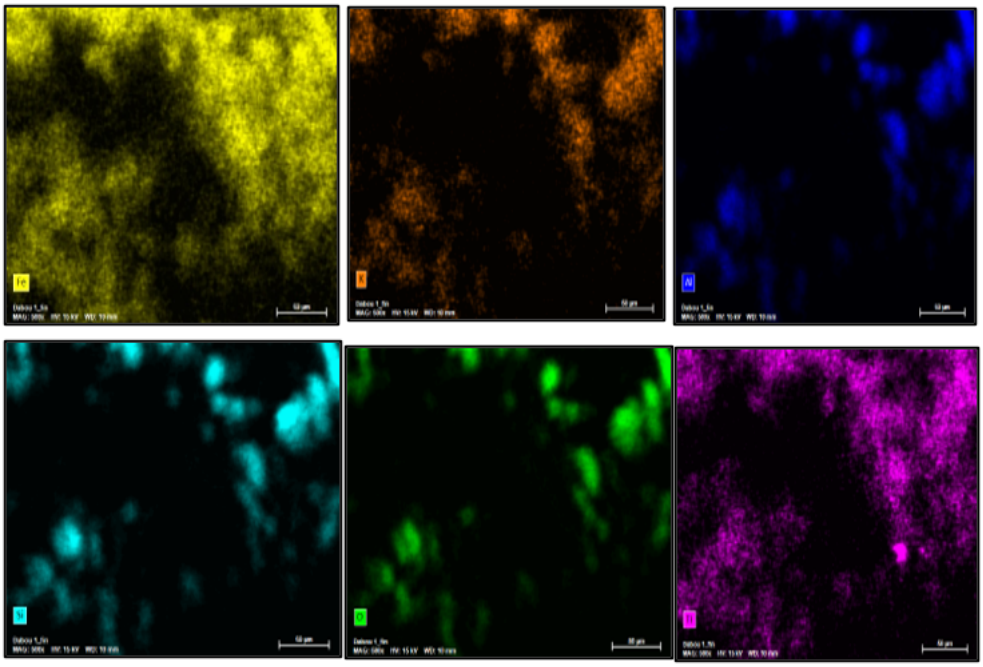

**Fig 2.** Mapping of the catalyst sample at 30 $\mu$m using BRUCKER EDS, model XFlash 30/100

## 3.4 Microanalysis quantification

The results of the 30 $\mu$m microanalysis in Figure 3 confirmed the presence of chemical element and that the sample contains 11.92% carbon (C), 49.41% oxygen (O), 12.93% aluminium (Al), 15.74% silica (Si), 9.22% iron (Fe) and 0.84% titanium (Ti).

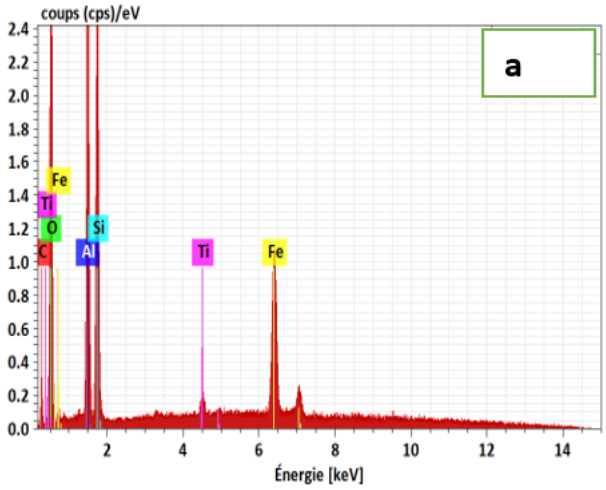


b

Dabou 1_fin

| Elément | A | Raie | Net | Mass. [%] | Mass. norm. [%] | Atom. [%] |
|---|---|---|---|---|---|---|
| C | 6 | K-Serie | 1444 | 12.00 | 11.92 | 18.71 |
| O | 8 | K-Serie | 20879 | 49.77 | 49.41 | 58.25 |
| Al | 13 | K-Serie | 21210 | 13.03 | 12.93 | 9.04 |
| Si | 14 | K-Serie | 21594 | 15.85 | 15.74 | 10.57 |
| Ti | 22 | K-Serie | 1569 | 0.84 | 0.84 | 0.33 |
| Fe | 26 | K-Serie | 15099 | 9.22 | 9.16 | 3.09 |
| | | | **Total:** | **100.72** | **100.00** | **100.00** |

**Fig 3.** Spectrum (a) and quantification (b) of the catalyst sample at 30 $\mu$m using BRUCKER EDS, model XFlash 30/100

## 3.5 X-ray diffractogram pattern of catalyst

As illustrated in Figure 4, the mineralogical analysis of the catalyst indicates that it is composed mainly of quartz ($SiO_2$), goethite ($\alpha$-FeO(OH)), kaolinite ($Al_2Si_2O_5(OH)_4$) and muscovite ($KA_{l2}(AlSi_3O10)(OH)_2$). The analysis primarily reveals the presence of an intense peak corresponding to quartz.

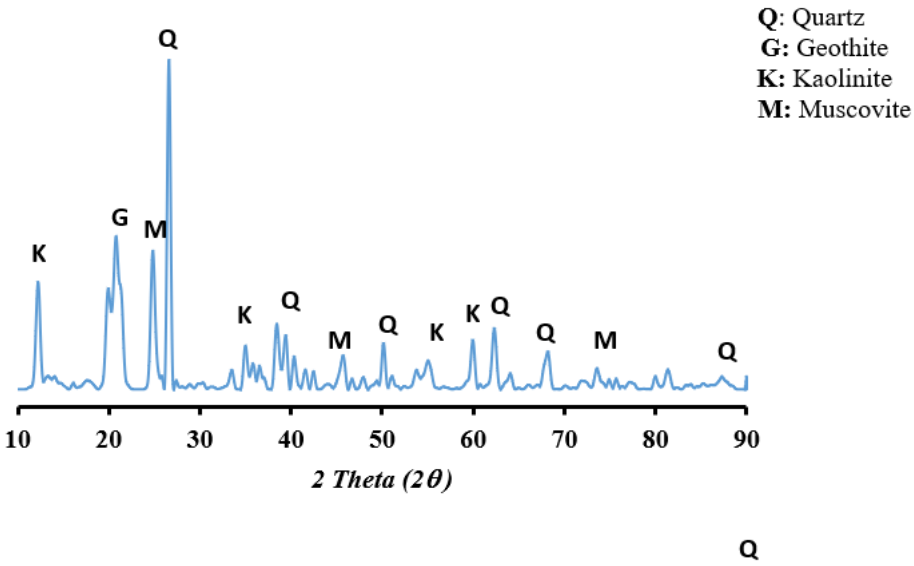


**Fig 4.** X-Ray diffractogram of catalyst

## 3.6 Langmuir and Freundlich models

As demonstrated in Figure 5, the linear forms of the Langmuir and Freundlich models are presented. It is evident that the Langmuir model provides a more accurate fit to the data when compared with the Freundlich model, as evidenced by the regression coefficient ($R^2$ = 0.9924) approaching unity. In accordance with the stipulations set out in the Langmuir model, the isotherm constant is determined to be 6.19 L $g^{-1}$, whereas that of freundlich is 0.936 L $g^{-1}$.

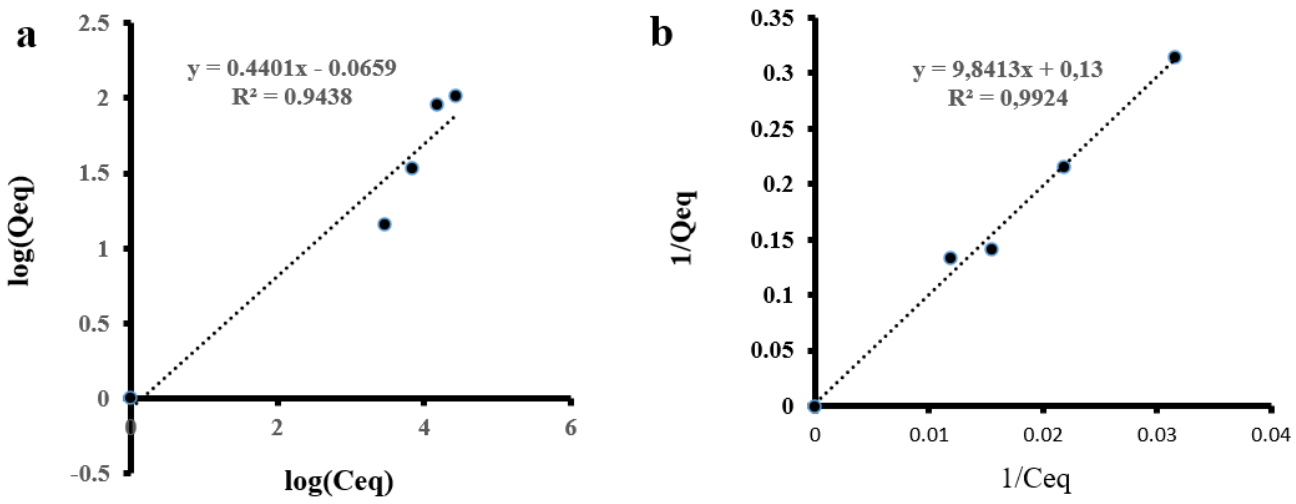


**Fig 5.** IC adsorption isotherms. a: Freundlich model, b: Langmuir model

### 3.7 Different degradation systems

As demonstrated in Figure 6, the degradation and adsorption kinetics of IC from different systems over time are shown. The IC/Cat system, which essentially represents adsorption, has an efficiency of 9.5%. In contrast, the Ox/Cat system has an efficiency of 13.73%. The combined systems demonstrate an efficiency of 26.36%, representing a 3.13% gain. With regard to the IC/Ox/US system, an efficiency of 40.15% was obtained. The addition of the catalyst to the system results in an efficiency of 61.35%, representing a 21.2% increase.

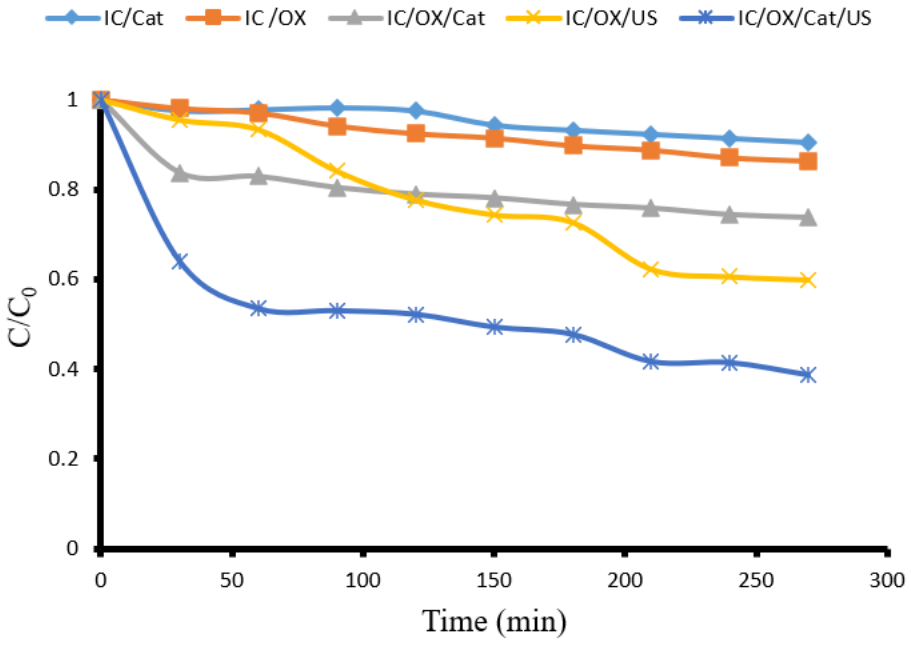


**Fig 6.** Kinetic degradation and adsorption of IC. Experimental conditions: [IC] =30 $\mu$M, [PS]=25 $\mu$M, catalyst dose = 2 g/L, pH = 6.45, reaction time 270 min

### 3.8 Degradation kinetic and second-order rate constant

The amounts of the pollutant, the oxidant and the catalyst were optimized by changing each one over time. The decay of organic compounds by radicals (R) is usually described as a second-order reaction [12]:

$$\frac{d\,[IC]}{dx} = -k\,[IC].[R] \quad \text{(Eqn. 2)}$$

In this equation, [R] denotes the steady-state concentration of the radicals, [IC] represents the concentration of IC in water, k is the second-order rate constant, and t is the reaction time.

It is assumed that the instantaneous concentration remains constant. In this case, the kinetics of the degradation of IC in water can be described using the pseudo-first-order equation given below:

$$[IC]t = [IC]_0^{-kapp\ .\ t} \quad \text{(Eqn. 3)}$$

In this study, the pseudo-first-order apparent rate constant (kapp) ($min^{-1}$) was calculated using linear regression of ln ($C_t/C_o$) versus time t. The resulting kapp ($min^{-1}$) was then plotted against [IC] or [PS] concentrations, as well as catalyst dose.

Indeed, the rate constant gets higher until 25 $\mu$M [IC], then gets lower very quickly after this concentration (See Figure 7a). As was the case in earlier experiments, the observed rate constant increased initially with increasing laterite load up to 2 g $L^{-1}$, and then decreased (See Figure 7b). Finally, the second-order kinetic constant increases with PS concentration from 10 to 25 $\mu$M, and decreases beyond this concentration (See Figure 7c). Consequently, the optimal amount of [PS], [IC] and catalyst dose was determined to be 25 $\mu$M, 30 $\mu$M and 2 g $L^{-1}$, respectively.

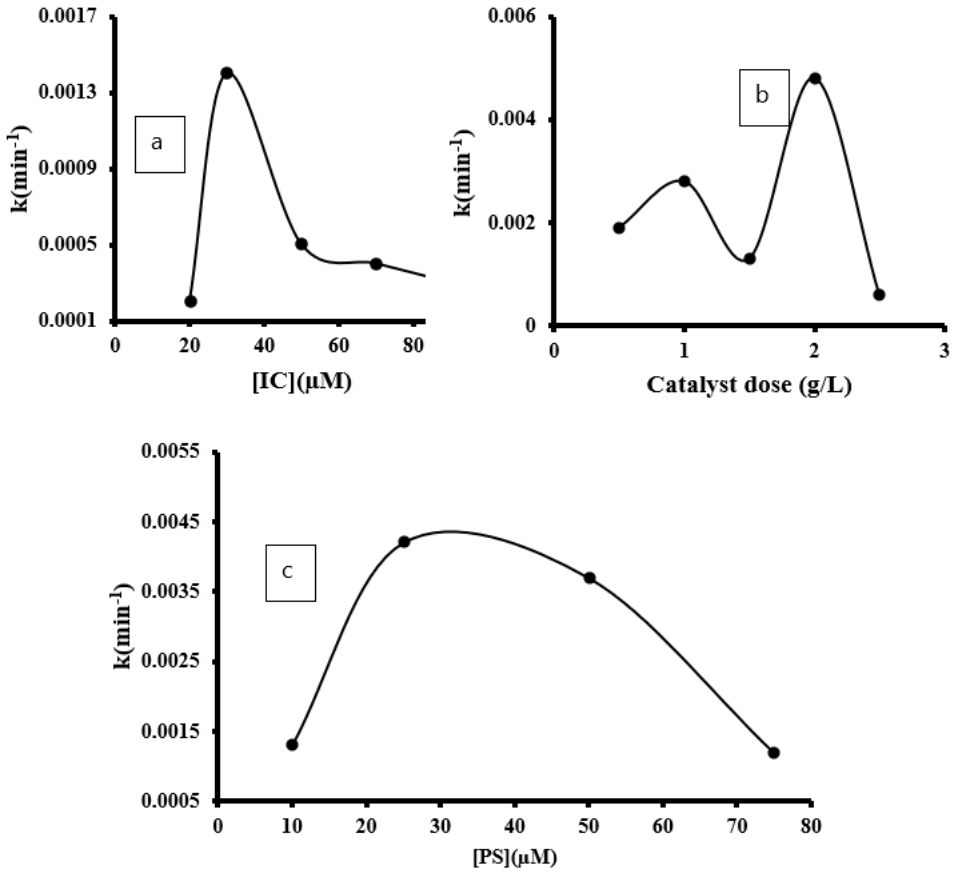


**Fig 7.** Rate constants as a function of [PS] (a), [IC] (b) and catalyst doses (c). Experimental conditions: [PS] = 10-75 $\mu$M, [IC] = 20-90 $\mu$M, catalyst dose = 0.5-2.5 g $L^{-1}$, pH = 6.45, Power US= 240 W, Frequency = 24 KHz, reaction time 270 min

### 3.9 IC amount trapped and implication radical

Figure 8 illustrates the involvement of radicals in the degradation process. Degradation of approximately 59.05%, 38.65% and 2.3% was observed in the presence of 1-4 Benzequinone (BQ), terbutanol (t-BuOH) and isopropanol (iPrOH), respectively, compared to degradation of 61.35% without scavenger. The use of BQ, t-BuOH and i-PrOH resulted in inhibition of 2.3%, 22.7% and 36.35%, respectively (Figure 8a). It can be assumed that the difference in inhibition (36.25%) observed when terbutanol and isopropanol were used separately corresponds to the contribution of the $SO_4^{\bullet -}$ radical. The relative contributions of $SO_4^{\bullet -}$, $OH^{\bullet}$, and $O_2^{\bullet -}$ to IC degradation are 59.25%, 37%, and 3. 75%, respectively (Figure 8b).

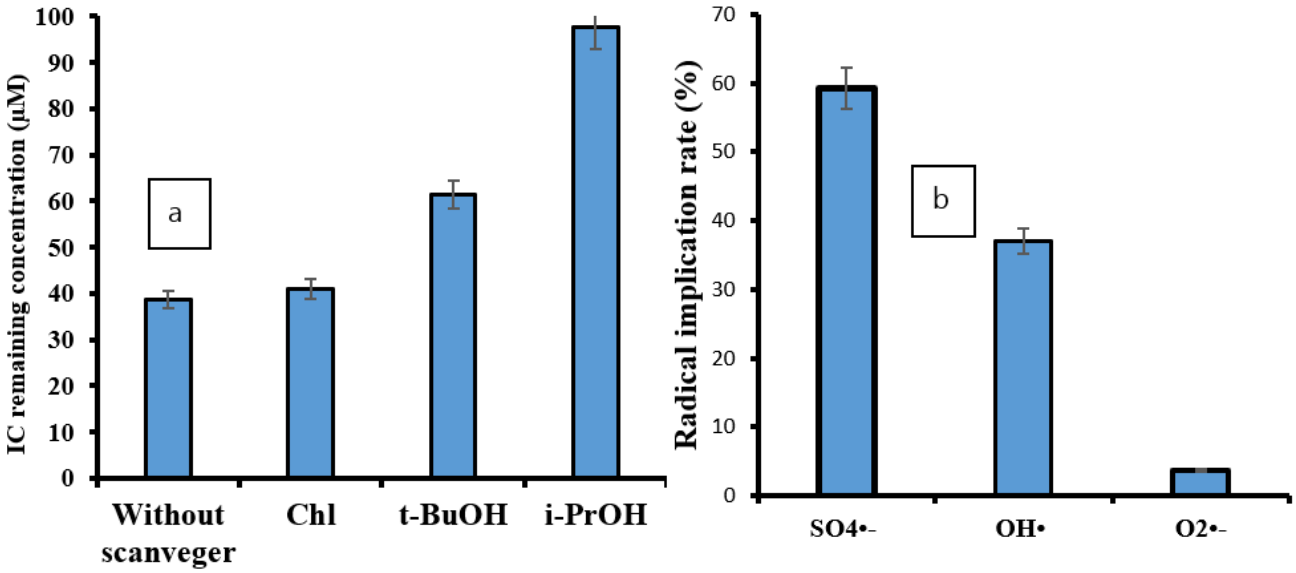


**Fig 8.** Scavenger's effect on degradation kinetic: Remaining concentration in the solution (a) and implication rates of each radicals (b). Experimental conditions: [PS] = 0.5 mM, [IC] = 40 $\mu$M, [Catalyst dose] = 0.2 g $L^{-1}$, pH = 6.45, Power US= 240 W, Frequency = 24 KHz, reaction time 270 min

The elemental composition of the catalyst has been analysed, and the results indicate that iron (Fe) and silica (Si) are the most abundant elements, at 28.98% and 59.13% respectively. These results are consistent with the XRD data, which also indicate a majority of iron oxide III ($Fe_2O_3$, 26.85%) and quartz ($SiO_2$, 57.34%). The presence of these elements was also confirmed through microanalyses. This outcome is consistent with those obtained by Atsé *et al.*[10], who utilised a catalyst from the same geographical area. The study of adsorption in terms of the equilibrium time effect demonstrates that the percentage of elimination increases with contact time until it reaches a constant value, characteristic of the state of equilibrium between the clay and the substance present in the aqueous solution. The high linearity of the straight lines, as indicated by a high regression coefficient $R^2$ of 0.99, suggests an excellent fit to the Langmuir model. Conversely, the Freundlich model appears to be less suitable, as evidenced by the linear regression coefficients. The Langmuir model suggested a monolayer of uniform molecules would cover the surface[12]. These values were generally less than one, which suggests that the clay was sticking to the surface[13]. Then, the addition of the catalyst to the system results in an efficiency of 61.35%, representing a 21.2% increase. The fact that clay and ultrasound irradiation work so well together is down to the increased generation of reactive oxygen species ($SO_4^{\bullet -}$, $OH^{\bullet}$, and $HO_2^{\bullet}/O_2^{\bullet -}$). The radicals in question are produced from persulfate activation in the context of redox cycling occurring at the interface between surface-bound $\equiv Fe^{III}$ and $\equiv Fe^{II}$ on clay, as has been previously documented in the extant literature[14]. The process is facilitated by sonication activity[14]. The following equation is derived:

$$\equiv Fe^{III+} + H_2O \longrightarrow \equiv Fe^{II+} + OH^{\bullet} + H^{+} \quad (1)$$

It has been shown that the production of $\equiv Fe^{II}$ can be accomplished by reducing $Fe^{III}$ sites found on the surfaces of laterite. After this, something else happens: the $Fe^{II}$ that was made reacts with PS, and $SO_4^{\bullet -}$ is formed. This is what happened next[15].

$$\equiv Fe^{II} + S_2O_8^{2-} \longrightarrow \equiv Fe^{III} + SO_4^{\bullet -} + SO_4^{2-} \quad k = 2.7 \times 10^1 M^{-1} s^{-1} \quad (2)$$

Then, another substance called $OH^{\bullet}$ can be produced when $SO_4^{\bullet -}$ reacts with $H_2O/HO^{\bullet}$ [16].

$$SO_4^{\bullet -} + H_2O \longrightarrow SO_4^{2-} + OH^{\bullet} + H^+ \quad k[H_2O] = 1.3 \times 10^3 s^{-1} \tag{3}$$

$$SO_4^{\bullet -} + OH^- \longrightarrow SO_4^{2-} + OH^{\bullet}(pH > 8.5) \quad k = 6.5 \pm 1 \times 10^7 M^{-1} s^{-1} \tag{4}$$

Finally, the combination of $SO_4^{\bullet -}$ and $OH^{\bullet}$ is also formed as a result of chain reactions, which are mostly controlled by the superoxide anion radicals ($O_2^{\bullet -}$) [16].

$$\equiv Fe^{II} + O_2 \longrightarrow \equiv Fe^{III} + O_2^{\bullet -} \tag{5}$$

Otherwise, the rate constant goes up from 20 to 25 $\mu$M and then down after this concentration (See Figure 3a). This is because there is a competition between IC and PS to interact with a certain number of active sites on solid surfaces. When there is a higher amount of IC, it can take over more of the $Fe^{III}$ spots, which then can't be used to make $Fe^{II}$ after being exposed to light or to interact with PS. This result matches earlier research that says how fast the reaction happens is limited when the catalyst or the surface sites are exposed to light, which starts the oxidation reaction [17], [18]. What's more, it has been shown that if there is more IC in the solution, fewer photons (particles of light) will enter the solution. This will reduce how well the ultrasound-assisted Fenton reaction works, as has been reported before [19]. As was seen in earlier experiments, the observed pseudo-first-order rate constant increased initially with increasing clay dose up to 2 g $L^{-1}$, and then decreased (See Figure 7b). This can be explained by the effects of screening, which occur when there are a lot of solid particles in a liquid, as has been previously reported for different types of ultrasound-Fenton reactions [20]. The rate constant increases up to 25 $\mu$M PS, then decreases quickly above this dose (See Figure 7c). This can be explained by the fact that PS can trap sulfate radicals and/or radical recombination at concentrations of over 25 $\mu$M of PS. Also, there might be a competition between IC and PS to see who can win over the radicals [21]. Firstly, it was hypothesised that i-PrOH would efficiently scavenge both generated $SO_4^{\bullet -}$ and $OH^{\bullet}$, due to the second-order rate constants of k i-PrOH, $SO_4^{\bullet -}$ (7.42 x $10^7$ $M^{-1}s^{-1}$) and k i-PrOH, $OH^{\bullet}$ (1.9 x $10^9$ $M^{-1}s^{-1}$). However, t-BuOH has been found to be more selective towards $OH^{\bullet}$ (k t-BuOH, $OH^{\bullet}$ = 6.0 x $10^8$ $M^{-1}s^{-1}$) than $SO_4^{\bullet -}$ (k t-BuOH, $SO_4^{\bullet -}$ = 8.31 x $10^5 M^{-1}s^{-1}$) [22], [23]. The radical scavenging percentage can then be calculated from the chemical concentration and the reactivity of the radicals with the IC. The addition of BQ to the PS/UVA/clay system resulted in a 2.3 % inhibition of IC degradation. BQ is notable for its ability to accept electrons from dissolved oxygen, effectively trapping the superoxide radical anion ($O_2^{\bullet -}$) with a high second-order rate constant (k BQ, $O_2^{\bullet -}$ = 9 x$10^8$ $M^{-1}$ $s^{-1}$) [24].

## 4 Conclusion

This work has demonstrated that the system, incorporating US/PS/iron-rich clay, is capable of effectively removing dyes from wastewater. This work achived the best conditions for PS, the pollutant, and the amount of catalyst. This produced the following results (i.e., [IC] = 30 $\mu$M, [PS] = 25 $\mu$M, [catalyst dose] = 2 g $L^{-1}$). So, 61.35 % of the degradation efficiency was seen under these best conditions. The degradation of IC was later found to be caused by $SO_4^{\bullet -}$, $OH^{\bullet}$ and $O_2^{\bullet -}$, with $SO_4^{\bullet -}$ being the main cause at 53.81%. This can be applied to work out how much $SO_4^{\bullet -}$, $OH^{\bullet}$ and $O_2^{\bullet -}$ contributed to the IC degradation (61.35%). It can be estimated that $SO_4^{\bullet -}$ contributed 55.95%, $OH^{\bullet}$ 34.16% and $O_2^{\bullet -}$ 9.89%. At the end of the fifth cycle, the efficiency of the degradation was recorded as a decrease to 5% more or less 2%. However, the TOC confirmed that the system was very stable, which was also shown by US/PMS/iron-rich clay. This shows that the mineralisation (i.e., 52 $\pm$ 2%) was good and did not change even after five oxidation cycles. This process system is an effective way to treat dyes in water. Thus, the current work is credited for a new process to remove dyes from water which is environmental friendly.

## 5 Acknowledgements

The APC, partially deferred by Indian Society for Education and Environment, is gratefully acknowledged.

The authors express their sincere gratitude to the University of Man, Côte d'Ivoire, for its financial support of the GEDEMONT project, which has made this study possible.

## References

1) Deshmukh SM, Dhokpande SR, Sankhe A, Khandekar A. Effluent wastewater technologies for textile industry: a review. *Reviews in Inorganic Chemistry*. 2025;45(1):21–40. https://doi.org/10.1515/revic-2024-0046.

2) Gupta S. A Review Study on Sustainable Dyes and Their Usage in the Fashion Industry. *International journal of research and analytical reviews*. 2024;11:63–72. https://doi.org/10.13140/RG.2.2.31385.22886.
3) Islam MM, Aidid AR, Mohshin JN, Mondal H, Ganguli S, Kumar A, et al. A critical review on textile dye-containing wastewater: Ecotoxicity, health risks, and remediation strategies for environmental safety. *Cleaner Chemical Engineering*. 2025;11:100165. https://doi.org/10.1016/j.clce.2025.100165.
4) Kumar A, Dixit U, Singh K, Gupta SP, Beg MSJ. Structure and properties of dyes and pigments. *Dye Pigment Applied Waste Treatment*. 2021;131. https://doi.org/10.5772/intechopen.97104.
5) Khan MI, Yahya SA, ElKhaleefa A, Shigidi I, Ali IH, Rehan M, et al. Toxic Anionic Azo Dye Removal from Artificial Wastewater by Using Polyaniline/Clay Nanocomposite Adsorbent: Isotherm, Kinetics and Thermodynamic Study. *Processes*. 2025;13:827. https://doi.org/10.3390/pr13030827.
6) Kumar JE, Sahoo MK. A review on effect of operational parameters for the degradation of azo dyes by some advanced oxidation processes. *Sustainable Chemistry for the Environment*. 2025;11:100274. https://doi.org/10.1016/j.scenv.2025.100274.
7) Moles S, Ormad MP, Gomez J, Szpunar J, Bolea E, Mosteo R. a Pilot plant approach combining photocatalysis and adsorption for antibiotics removal from slaughterhouse and urban wastewater treatment plant effluents. *Environment Technology Innovation*. 2024;34:103586. https://doi.org/10.1016/j.eti.2024.103586.
8) Moreno-Bermedo L, Correa-Puerta J, González-Fuentes C, Escalona N, Onfray C, Thiam A. Tea Waste as a Sustainable Catalyst Support for Enhanced Removal of Contaminants of Emerging Concern via the Electro-Fenton Process: A Circular Economy. Applied Science Approach. *Applied Sciences*. 2025;15:1418. https://doi.org/10.3390/app15031418.
9) Samianifard SM, Kalaee M, Moradi O, Mahmoodi NM, Zaarei D. Novel Biocomposite (Starch/Metal–Organic Framework/Graphene Oxide): Synthesis, Characterization and Visible Light Assisted Dye Degradation. *Journal of Photochemistry and Photobiology A: Chemistry*. 2024;450:115417. https://doi.org/10.1016/j.jphotochem.2023.115417.
10) Atsé WA, Essi MMM, Doubi BIHG, Kamagaté M, Aké AP, Kouamé AN. Physico-Chemical Characterization of Two Dabou Clays with a View to Use Them in the Treatment of Dyeing Wastewater. *Journal of Minerals and Materials Characterization and Engineering*. 2022;10(6):505–517. https://doi.org/10.4236/jmmce.2022.106036.
11) Adejumoke AI, Bankole DT, Pamela S, Temitope SA, Adewale FL. The efficiency of Raphia hookeri adsorbent in indigo carmine dye removal: Economy depth via chemometrics. *Heliyon*. 2024;10(11):e32121. https://doi.org/10.1016/j.heliyon.2024.e32121.
12) Faiq FK, Karar AA. Adsorption of Indigo Carmine Dye on Chitosan Grafted Poly (Methyl Methacrylate). 2024. https://doi.org/10.21123/bsj.2024.10316.
13) Wan JH, Zaoui A. Mechanical resistance behind fiber-reinforced polymer pile: Role of clay minerals. *Computers and Geotechnics*. 2024;168:106158. https://doi.org/10.1016/j.compgeo.2024.106158.
14) Kianian S, Toulakani RM, Zisti F, Balarak D, Siddiqui SH, Saloot MK. Degradation of Antibiotics by Ultrasound-Assisted Heterogeneous Activation of Persulfate and Peroxymonosulfate: A Review. *International Journal of Pharmaceutical Investigation*. 2023;14:23–29. https://doi.org/10.5530/ijpi.14.1.4.
15) Li G, Zhang Y, Zhang X, Zhang J, Sun B. Deciphering the Formation of Fe(IV) in the Fe(II)/Peroxydisulfate Process: The Critical Role of Sulfate Radical. *Environmental Science & Technology*. 2024;58(35):15864. https://doi.org/10.1021/acs.est.4c06675.
16) Guo Y, Zhang Y, Yu G, Wang Y. Revisiting the Role of Reactive Oxygen Species for Pollutant Abatement during Catalytic Ozonation: The Probe Approach versus the Scavenger Approach. *Applied Catalysis B Environmental*. 2021;280. https://doi.org/10.1016/j.apcatb.2020.119418.
17) Gao J, Alsaab HO, Zare MH, Shirazian S. Magnesiothermal reduction and doping strategies in engineered TiO2 for pharmaceutical degradation and CO2 conversion. *Clean Water*. 2025;8:76. https://doi.org/10.1038/s41545-025-00508-9.
18) Kamagate M, Coulibaly NG, Koffi APM, Zie O, Coulibaly L, Assadi AA, et al. Enhancing Levofloxacin Degradation in Contaminated Water: Catalytic Performance of Pegmatite in a Sodium Percarbonate/Ultrasound System. *Catalysts*. 2025;15. https://doi.org/10.3390/catal15040363.
19) Zeghioud H, Kamagate M, Coulibaly LS, Rtimi S, Assadi AA. Photocatalytic Degradation of Binary and Ternary Mixtures of Antibiotics: Reactive Species Investigation in Pilot Scale. *Chemical Engineering Research and Design*. 2019;144:300–309. https://doi.org/10.1016/j.cherd.2019.02.015.
20) Galeas S, Guerrero VH, Pontón PI, Goetz V. Visible Light-Driven Phenol Degradation via Advanced Oxidation Processes with Ferrous Oxalate Obtained from Black Sands: A Kinetics Study. *Molecules*. 2025;30:2059. https://doi.org/10.3390/molecules30092059.
21) Li G, Zhang Y, Zhang X, Zhang J, Sun B. Deciphering the Formation of Fe(IV) in the Fe(II)/Peroxydisulfate Process: The Critical Role of Sulfate Radical. *Environmental Science & Technology*. 2024;58(35):15864. https://doi.org/10.1021/acs.est.4c06675.
22) Li L, Zheng D, Gu X, Sun C, Liu Y, Dong W, et al. Mechanism of the improved Fe(III)/persulfate reaction by gallic acid for ibuprofen degradation. *Environmental Pollution*. 2022;314:120318. https://doi.org/10.1016/j.envpol.2022.120318.
23) Xiao S, Ma L, Wenhui A. Stability optimization of iron-based catalysts: Application of Cr-enriched alloy steel catalyst in ozonation pharmaceutical wastewater. *Separation and Purification Technology*. 2025;354:5. https://doi.org/10.1016/j.seppur.2024.129007.
24) Cai L, Yao Q, Du X, Tao X, Zou M, Zhou J, et al. Identification of Superoxide Contribution through the Quenching Method and Model System. *Environmental Science & Technology*. 2024;4(9). https://doi.org/10.1021/acsestengg.4c00187.